

Vishal Tandon<sup>1</sup>  
Brian J. Kirby<sup>2</sup>

<sup>1</sup>Department of  
Biomedical Engineering,  
Cornell University,  
Ithaca, NY, USA

<sup>2</sup>Sibley School of Mechanical  
and Aerospace Engineering,  
Cornell University,  
Ithaca, NY, USA

Received October 2, 2007  
Revised December 5, 2007  
Accepted December 5, 2007

## Review

# Zeta potential and electroosmotic mobility in microfluidic devices fabricated from hydrophobic polymers: 2. Slip and interfacial water structure

We discuss the structure of water at hydrophobic interfaces from the standpoint of its impact on electrokinetic phenomena in microfluidic devices fabricated from hydrophobic polymers such as Teflon® or Zeonor®. Water structuring at hydrophobic interfaces has been described as a source of interfacial charge (see Part 1, this issue), and dewetting phenomena, whether *via* depletion layers or nanobubbles, contribute to slip and enhanced apparent electrokinetic potentials. Issues concerning the impact of hydrodynamic slip and the role of diffuse interfacial structures are discussed. These issues are coupled with each other and with interfacial charge concerns, providing challenges for measurements of individual parameters.

### Keywords:

Electrokinetic / Electroosmosis / Hydrophobic / Slip / Zeta potential

DOI 10.1002/elps.200800735

## 1 Introduction

Water is among the most intriguing of materials. In addition to its ubiquity and engineering relevance, water poses challenges owing to the complexity of its interactions with itself, solutes, and interfaces. These complexities have made it difficult to define molecular models for water that predict all important phenomena.

The presence of a solid interface interferes with the structure of water's hydrogen-bonded lattice. For hydrophilic surfaces, this can lead, for example, to orientation of water dipoles [2] and an attendant reduction in electrical permittivity [3]. For hydrophobic surfaces, the results are not as well understood. The structure of water at hydrophobic interfaces may be a driving factor for interfacial charge, and it is closely related to observed hydrodynamic slip.

When considering the influence of hydrophobic surfaces on electrokinetic phenomena, we focus on those aspects of interfacial structure that affect the fluid mechanical problem, namely the actuation of mobile charge (the key source term in the hydrodynamic equations), and the influence on

hydrodynamic slip (the boundary condition for the hydrodynamic equations). Study of electrokinetics in hydrophobic substrates is more complicated than in hydrophilic substrates because (i) modes of charge formation at the fluid-solid interface are less well-understood [1] and (ii) the hydrodynamic slip boundary condition is highly coupled with macroscopically observable electrokinetic phenomena, leading to inflated apparent electrokinetic potentials. Modeling slip is non-trivial since the origin of slip is also currently in dispute [4]. Both slip and surface charge have been postulated to depend on the molecular/supramolecular structure of water at the hydrophobic interface; proposed structures include ice-like hydrogen-bonded networks of water molecules [5–7], regions of depleted water density [8], and nanobubbles [9].

In the companion to this paper [1], we have presented fundamental electrokinetic relations and then discussed different models for the origins of charge on hydrophobic surfaces, most of which have few if any charged surface groups. Here, we discuss slip phenomena and interfacial molecular/supramolecular structures. As was the case in [1], we focus on microfluidic devices with aqueous electrolyte solutions, and exclude discussion of large amphiphathic and organic surfactants.

## 2 Electrokinetics

Here we consider electrokinetic phenomena following the notation and discussion presented in [1]. We assume that charge separation phenomena lead to a net charge at the

**Correspondence:** Dr. Brian J. Kirby, 238 Upson Hall, Cornell University, Ithaca, NY 14853, USA

**E-mail:** BK88@cornell.edu

**Fax:** +607-255-1222

**Abbreviations:** **AFM**, atomic force microscopy; **ATR-FTIR**, attenuated total reflection Fourier transform infrared; **EDL**, electrical double layer; **MD**, molecular dynamics; **OTS**, octadecyl trichlorosilane; **PIV**, particle image velocimetry; **SFA**, surface force apparatus; **SFG**, sum frequency generation

interface between the aqueous solution and the microdevice substrate, and that charge coincides with an interfacial potential (the zeta potential,  $\zeta$ ) as well as a diffuse electrical double layer that can be described with a Gouy-Chapman-Stern model [10]. The electrical potential distribution is given by the Poisson-Boltzmann equation:

$$\nabla^2 \psi = -\frac{\rho_e}{\epsilon} = -\frac{1}{\epsilon} \sum_i n_{0,i} e z_i \exp\left(-\frac{e z_i}{k_B T} \psi\right) \quad (1)$$

and nondimensionalization of the Poisson-Boltzmann equation leads to the Debye length  $\lambda_D$ :

$$\lambda_D = \sqrt{\frac{\epsilon k_B T}{2e^2 (\Gamma/2)}} \quad (2)$$

We interpret the effects of interfacial phenomena at hydrophobic surfaces primarily in the context of electroosmosis and streaming potential. Electroosmosis is described in the Smoluchowski limit by the electroosmotic mobility,  $\mu_{EO}$ , given by

$$\mu_{EO} = -\frac{\epsilon \zeta}{\eta} \quad (3)$$

while streaming potential in the Debye-Hückel, thin double layer, and Smoluchowski limits is given by

$$\Delta \phi = -\frac{\epsilon \zeta}{\eta \sigma} \Delta P. \quad (4)$$

Our focus in this paper is deviation from Smoluchowski-type relations such as Eq. (4).

### 3 Slip boundary condition at water-hydrophobe interfaces

In most physical descriptions of microfluidic systems, no-slip boundary conditions at solid-liquid interfaces are assumed [20, 21]. Flows in hydrophobic microfluidic systems, however, have been shown to deviate from those predicted by models using no-slip boundary conditions [4, 22, 39]. Here, we focus on slip in hydrophobic systems with careful attention to electrokinetically driven flow.

#### 3.1 Quantifying slip

Navier [10] and later Maxwell [41] proposed a linear boundary condition which remains as the standard description of slip. In this formalism, the fluid velocity field component tangent to the surface,  $u_t$ , is proportional to the shear rate at the surface.

$$u_t = b \mathbf{n} \cdot (\nabla \mathbf{u} + \nabla \mathbf{u}^T) \cdot (1 - \mathbf{n} \mathbf{n}) \quad (5)$$

where  $u_t$  is the slip velocity,  $\mathbf{u}$  is the fluid velocity field,  $b$  is the slip length parameter, and  $\mathbf{n}$  is the unit vector normal to the wall. In a simpler form,

$$u_t = b \left( \frac{\partial u_t}{\partial n} \right)_{\text{wall}} \quad (6)$$

where the differential length  $\partial n$  is in the direction normal to the wall. Here the proportionality constant,  $b$ , has the units of length, and is referred to as the slip length. The slip length can be interpreted as representing the distance beyond the wall at which the fluid velocity field becomes zero, if the velocity field is extrapolated linearly (Fig. 1). Physically, the slip length is analogous to a surface friction coefficient, as it relates a field property (shear rate) to the boundary condition. Typically, experimental measurements of slip are reported as slip lengths.

#### 3.2 Measurement of slip in microsystems

Slip lengths can be measured directly or inferred through measurements of the macroscopic properties of a microfluidic system. In order for slip to have a significant and measurable effect on the macroscopic properties of a system, the slip length should approach the same order as the characteristic length scale for the system (roughly the length over which fluid velocity in the bulk solution changes to the value at the wall). There is a great deal of variation in slip length measurements, and we do not attempt to list slip lengths for various materials here (see [4] for a summary of slip length measurements). In hydrophobic materials, slip lengths are typically on the order of nanometers, though some have recorded slip lengths of microns [29, 30]. In electroosmotic flow, the characteristic length, the Debye length, is typically on the order of nanometers, so slip can have a very significant impact on bulk flow properties.

Several observables have been used to infer slip properties, including the flow rate-pressure relation in a channel, drainage forces observed between surfaces moved in relation to each other, and electrokinetic phenomena. One standard indirect method for measuring slip is to apply a known pressure gradient across a channel and measure the flow rate

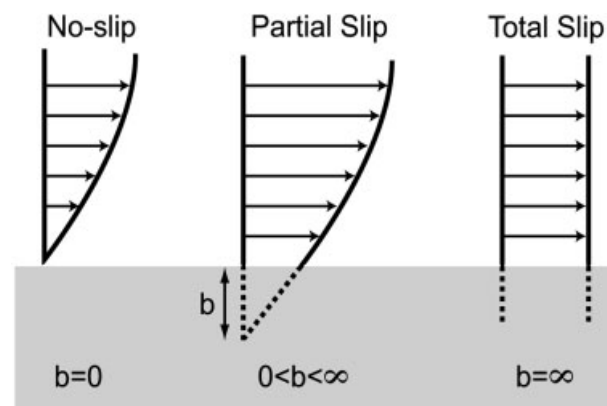


Figure 1. Scheme showing an interpretation of the slip length,  $b$ .

[23, 25, 42–44]. Slip in the system will lead to a larger flow rate than that expected from a model based on the no-slip boundary condition. For a circular microchannel,

$$\frac{Q(b)}{Q_{NS}} = 1 + \frac{4b}{a} \quad (7)$$

where  $Q$  is the slip flow rate,  $Q_{NS}$  is the flow rate if no-slip is assumed, and  $a$  is the radius of the channel. Another macroscopic technique involves measuring the viscous force opposing the drainage of a liquid film between hydrophobic surfaces [26, 45–49] and comparing to theoretical models [8, 50–53]. The presence of slip in the system reduces the apparent viscous resistance to draining. Two techniques for measuring drainage force have been developed; the surface force apparatus (SFA) and atomic force microscopy (AFM). The SFA was originally invented to measure van der Waals forces through a gas [54], but was adapted to measure forces between solids immersed in liquids by Israelachvili *et al.* [45]. An SFA uses interferometry to measure the distance between a stationary solid surface and a mobile one, and a spring attached to the mobile surface to measure the force acting on the surfaces. The SFA is now routinely used for measurements of slip length [32]. In AFM, a colloidal sphere attached to a flexible cantilever with known mechanical properties is brought in close proximity to a surface, and the deflection of the cantilever is measured [22, 34, 37]. Sedimentation has also been used to measure slip [22], where colloids experiencing slip sediment faster than expected.

Electrokinetic phenomena result in macroscopically observable quantities that are expected to be largely affected by slip, due to the localization of shear to the double layer, which is typically small as compared to the dimensions of a microchannel. Churaev *et al.* [24] used streaming potential to study slip in methylated quartz capillaries. Streaming potentials measured in the presence of slip are expected to be larger than those measured in the absence of slip (see Section 3.4, specifically Eq. 11). When compared to traditional techniques, there is a key problem with electrokinetic observation, which limits its use in measurement of slip. Streaming potential and electroosmosis are both functions of two unknowns that are difficult to measure independently: the electrokinetic potential,  $\zeta$ , and the slip length,  $b$ . In order to get an estimate of  $\zeta$ , Churaev *et al.* used a non-ionic trisiloxane surfactant to render their methylated quartz hydrophilic, claiming that the surfactant influenced the surface potential only weakly, and made the surface no-slip. Precise measurements of slip lengths through electrokinetic observation, however, require either a method for measuring the  $\zeta$ -potential that is unaffected by slip, or a combination of techniques that are affected by slip differently.

Various velocimetry techniques have been used for measuring slip at the solid-liquid interfaces more directly. In particle image velocimetry (PIV), passive tracer particles are added to the flow and observed optically [27, 29, 30, 55]. In microfluidics applications, the tracer particles can be hun-

dreds of nanometers in diameter, and the technique is referred to as micro-PIV [27, 29, 30]. The resolution of micro-PIV is limited by the depth of field of the observation optics, and since tracer particles must be small enough to negligibly affect the flow field, errors may be introduced from particle diffusion, which must be corrected in post processing [29, 30]. Evanescent field illumination has been utilized in order to increase the resolution of PIV, in which case the technique is referred to as nano-PIV [55, 56]. When using velocimetry methods to observe electroosmotic flow, it is important to take the electrophoretic mobility of the tracer particles into account [56].

### 3.3 Dependence of slip on physical parameters

The origin of slip in microfluidic systems is not well understood. In general, hydrophilic systems have been shown to have very small or negligible slip lengths [26, 28, 48, 49], while hydrophobic systems have significant slip [22–39]. Although the slip length does systematically increase with hydrophobicity of the substrate, it is only weakly correlated with its contact angle [4]. Examining the dependence of slip on a variety of physical parameters can help in understanding how the surface properties of hydrophobic substrates lead to the generation of slip.

Molecular dynamics simulations [57] and experiments [38, 49, 58] have shown that roughness tends to decrease slip. This is critical because microfluidic devices are usually the product of chemical etches (on glass or silicon) and/or templated synthesis (soft lithography, hot embossing, injection molding, replica molding, *etc.*), and these processes typically lead to a surface that is rough on the atomic level. Results on atomically-smooth mica [37, 45, 58] or even organosilane-modified Si wafers [59–63] may not be representative of the results on microfluidic substrates, nor can colloidal results with oil droplets be assumed to be representative of the roughness expected on the surfaces of microfluidic devices. Roughness induces local flows which lead to viscous dissipation of mechanical energy; essentially the same mechanism which leads to the no-slip boundary condition in typical flows. A number of experiments have also shown slip to depend on the shear rate ( $b = b(\dot{\gamma})$ ) [23, 25, 26, 38, 39, 64–67], in which case Eq. (6) is non-linear. Models that have been developed for shear-dependent slip are often based on the postulate that a layer of gas bubbles exists at the interface [8, 68–72]. A layer of gas in between the bulk solution and the solid channel wall has in general a non-zero velocity at the fluid-fluid interface, which defines a local apparent slip length as

$$b = h \left( \frac{\eta_1}{\eta_2} - 1 \right) \quad (8)$$

where  $h$  is the thickness of the low viscosity layer,  $\eta_1$  is the bulk solution viscosity and  $\eta_2$  is the viscosity of the gas layer. Some slip measurements are unsteady, which means that

the size of the gas/bubble layer will be a function of the instantaneous pressure distribution in the fluid. As is the case with interfacial charge formation, the structure of water at the interface can have a large effect on slip (see Section 4).

Slip has been shown to depend on the type and quantity of dissolved gas in solution [22, 73, 74], supporting the notion of nanobubbles or a region of depleted water density at fluid-hydrophobe interfaces. In [22], Boehnke *et al.* demonstrated that (1) solvophilic beads had sedimentation velocities that were not a function of dissolved gas and (2) beads in degassed solution had sedimentation velocities that were not a function of the solvophilic/solvophobic nature of the material; however, they showed that solvophobic beads in solutions in contact with air had higher sedimentation velocities than the same system in contact with vacuum. Using an SFA to study a tetradecane interface, Granick *et al.* [73] showed that a system saturated with CO<sub>2</sub> obeyed no-slip boundary conditions, while a system saturated with Ar deviated significantly from no-slip. This can be explained by specific bonding of CO<sub>2</sub> with H<sub>2</sub>O, which differentiates it from other gases such as Ar, N<sub>2</sub>, and O<sub>2</sub>, and is also responsible for the anomalously high solubility of CO<sub>2</sub> [75–77]. With PIV experiments, Tretheway *et al.* [74] measured the slip length as a function of absolute pressure, and showed that the measured slip length decreases with increasing absolute pressure. From these observations, it is clear that dissolved gases influence slip phenomena, though the mechanism by which it occurs is unclear (to be discussed more in Section 4).

### 3.4 Slip in electrokinetic systems

If the slip boundary condition given by Eq. (6) is applied to electroosmotic flow, then in the Debye-Hückel limit with uniform fluid properties, the resulting electroosmotic velocity,  $u_{EO}$  is

$$u_{EO} = -\frac{\varepsilon E}{\eta} \zeta(1 + b^*) \quad (9)$$

where  $b^* = b/\lambda_D$  is the slip length normalized by the Debye length. Similarly, in pressure driven flow, the streaming potential with the slip boundary condition becomes [24]

$$\Delta\phi = -\frac{\varepsilon\Delta P}{\eta\sigma} \zeta(1 + b^*) \quad (10)$$

where once again the Debye-Hückel limit and spatially uniform solution conductivity have been assumed. In both cases, if the effect of slip is ignored, the measured or apparent zeta potential,  $\zeta_a$ , inferred from electrokinetic measurements will be larger than the potential drop across the EDL.

$$\zeta_a = \zeta(1 + b^*) \quad (11)$$

The Debye parameter,  $\lambda_D$ , can be quite small (~ 10 nm when the counterion concentration is 1 mM), so slip can have a

significant effect on electrokinetic systems. Since slip leads to an effective  $\zeta$ -potential that has precisely the same form in both the electroosmotic velocity and the streaming potential, measurements of these two quantities cannot be used to infer both the slip length and the  $\zeta$ -potential in the Debye-Hückel limit. In order to decouple the slip length parameter from the  $\zeta$ -potential, either a  $\zeta$ -potential measurement which is not affected by slip, or an independent measurement of the slip length is necessary.

In the Debye-Hückel limit, Yang and Kwok have expanded this result for infinite flat plates. They have reported *via* an analytical result for thin double layers [78] that an additional correction term needs to be added, which accounts for the relative increase in flow-induced ion transport (current) attendant with increasing slip:

$$\zeta_a = \frac{\zeta(1 + b^*)}{1 + \frac{b}{a} \frac{\varepsilon}{\eta D} \zeta^2} \quad (12)$$

where  $2a$  is the distance between the plates and  $D$  is the diffusivity of the ions. Relaxing the thin DL limit, they have reported results numerically for flat plates [79], circular channels [80], and rectangular channels [81], with qualitatively similar results.

In the presence of slip, the errors introduced by linearizing the Poisson-Boltzmann as in Eq. (9) can be quite large. It is illustrative to examine the full non-linear Poisson Boltzmann equation for the case of a symmetric  $z:z$  electrolyte on a flat plate with a given  $\zeta$ -potential. The apparent zeta potential,  $\zeta_a$ , now takes the form

$$\zeta_a = \zeta \left[ 1 + b^* \frac{2}{z\zeta^*} \sinh\left(\frac{z\zeta^*}{2}\right) \right] \quad (13)$$

where  $\zeta^* = \frac{\zeta}{k_B T/2}$ . Apparent  $\zeta$ -potentials are plotted in Fig. 2 for a variety of parameters. It is clear from all of the plots in Fig. 2 that the linearized solution fails as  $\zeta$  increases. In addition, the non-linear Poisson-Boltzmann equation introduces a dependence on the valence of the electrolyte,  $z$ , which is not present in the linearized solution. Comparison of Fig. 2a to Fig. 2b (or Fig. 2c to Fig. 2d) shows that the Debye-Hückel approximation becomes worse for ions of larger valence. Finally, Figs. 2c and 2d show that the Debye-Hückel approximation becomes worse as the slip length increases.

For cases of a general electrolyte solution, Eq. (1) must be solved numerically. Numerical results for an electrolyte with a 2:1 ratio of monovalent anions to divalent cations are shown in Fig. 3. Interestingly, the ratio  $\zeta_a/\zeta$  goes through a minimum as a function of  $\zeta$  for large enough slip lengths. This simple analysis demonstrates that the presence of slip in electrokinetic systems can lead to large deviations from no-slip behavior. It should be noted, however, that this analysis assumes a constant slip length to facilitate analytical treatment. At present, the true nature of slip and its dependence on input parameters is largely unknown.

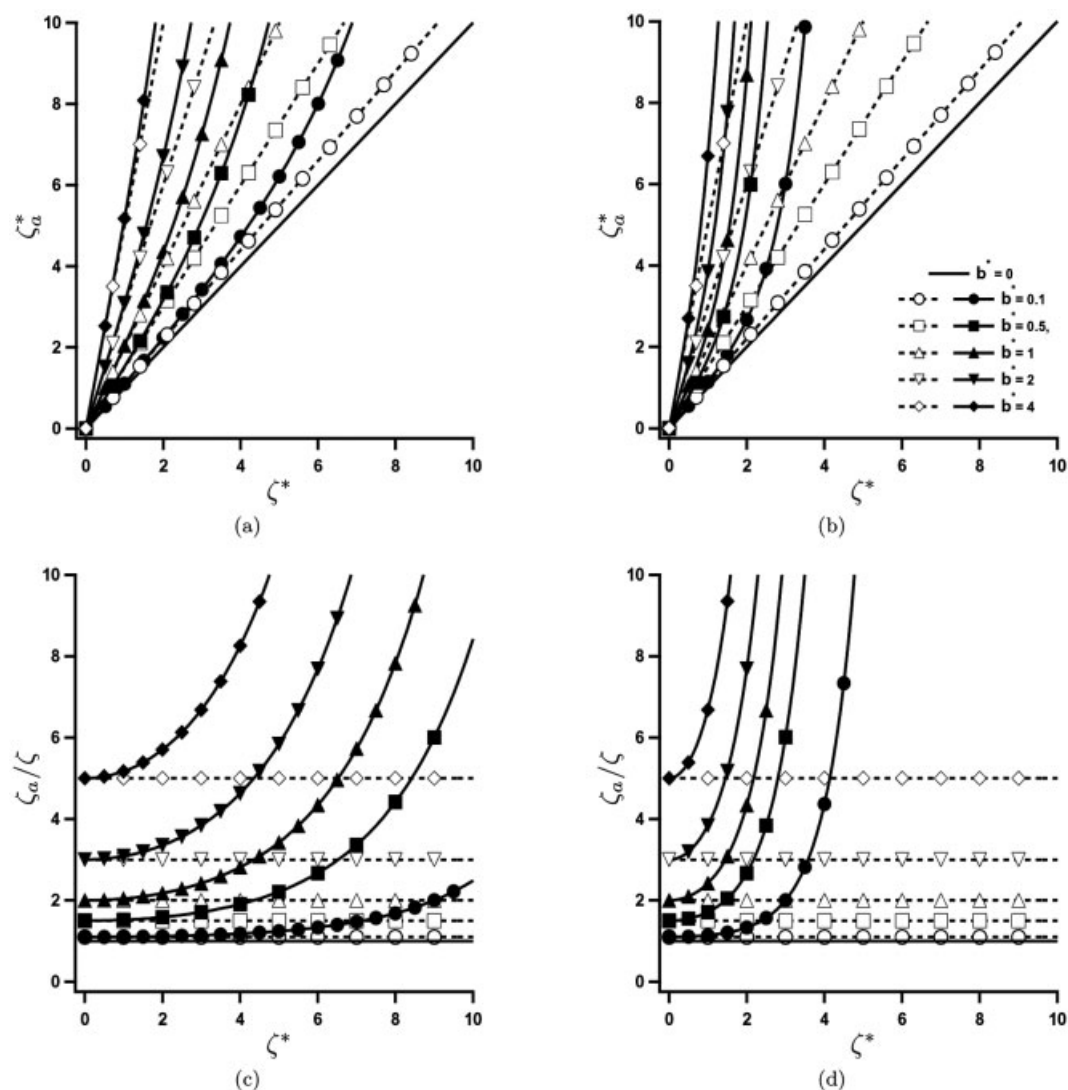


**Figure 2.** Plots of (a)  $\zeta_a^*$  vs.  $\zeta^*$  for a 1:1 electrolyte, (b)  $\zeta_a^*$  vs.  $\zeta^*$  for a 3:3 electrolyte, (c)  $\zeta_a/\zeta$  vs.  $\zeta^*$  for a 1:1 electrolyte, and (d)  $\zeta_a/\zeta$  vs.  $\zeta^*$  for a 3:3 electrolyte. Closed symbols and solid lines correspond to the nonlinear solution to the Poisson-Boltzmann Equation (Eq. 13). Open symbols and dashed lines correspond to the Debye-Hückel approximation (Eq. 9).  $\zeta_a^* = \zeta_a/k_B T/e$  and  $\zeta^* = \zeta/k_B T/e$ . For reference,  $k_B T/e$  at room temperature (293K) is 25 mV.

Few experiments directly addressing the effects of slip in electrokinetic systems have been conducted. As discussed earlier, Churaev *et al.* [24] used streaming potential measurements in an attempt to infer the slip length for methylated quartz in aqueous solution. They used a surfactant to render the substrate hydrophilic, and claimed that the modified quartz gave a good estimate for the true (slip-free)  $\zeta$ -potential. This is at best an estimate, however, and in general it is very difficult to decouple  $b$  from  $\zeta$ .

MD simulations of electrokinetics in hydrophobic microfluidic channels at finite temperature predict a breakdown of the Boltzmann approximation assumed in Eq. (1) [82]. Ion concentration distributions oscillate near the fluid-solid interface, in a manner consistent with some modified

Poisson-Boltzmann approaches. The immobile Stern layer of charges is present in hydrophilic surfaces, but absent in hydrophobic surfaces. Motion of ions near the interface results in slip in the hydrophobic case, which is well-described by Eqs. (6) and (9). In [82] Joly *et al.* chose to describe charge interaction *via* an effective dielectric media. This description was very successful in demonstrating the role of condensed ion layers effects in slip, though full atomistic simulation of the water molecules may be necessary in order to understand the interplay between slip and charge formation at the interface. Such a simulation is very challenging, since electrostatic interactions are long range, and computations of long range pair potentials for significant numbers of molecules are very costly.

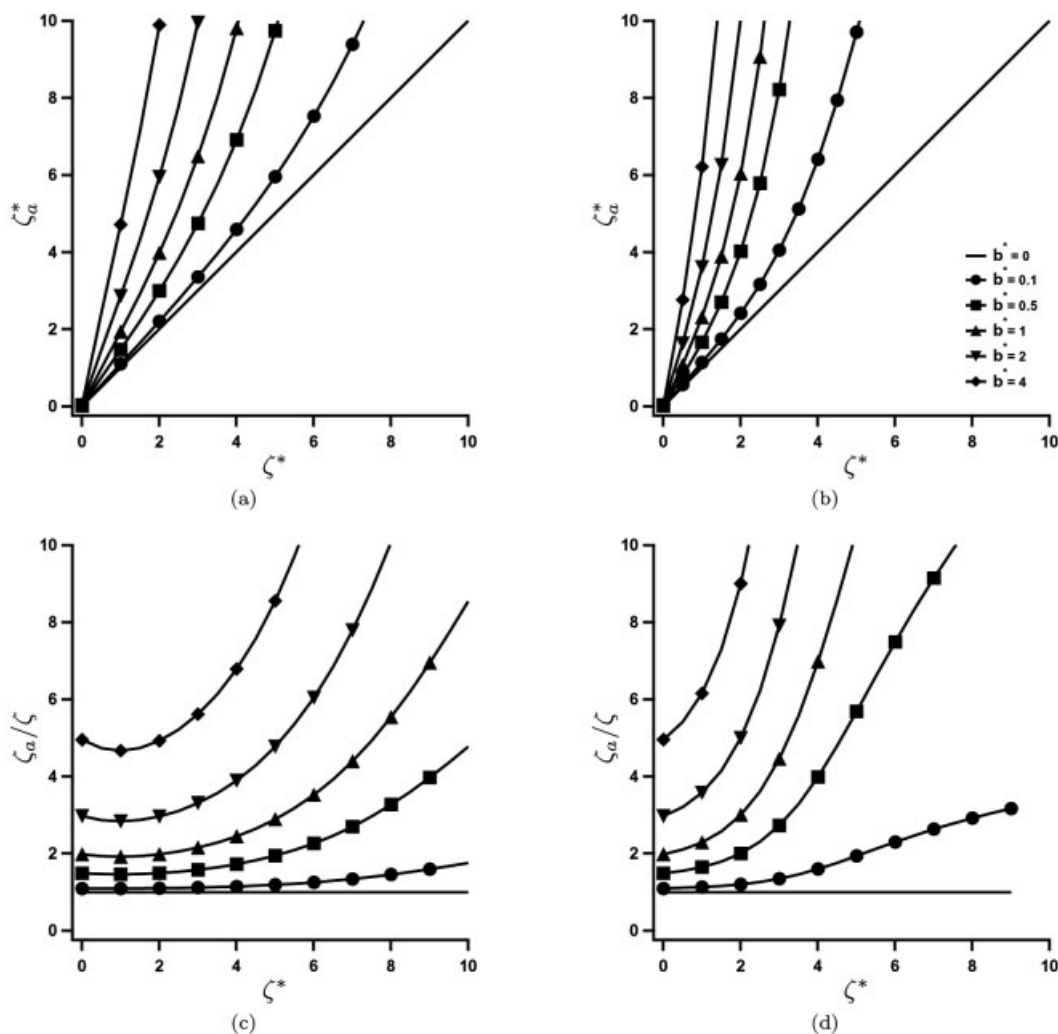


**Figure 3.** Numerical solutions to Eq. 1 for a 2:1 ratio of monovalent anions to divalent cations over a flat plate. (a)  $\zeta_a^*$  vs.  $\zeta^*$  for a positively charged plate, (b)  $\zeta_a^*$  vs.  $\zeta^*$  for a negatively charged plate, (c)  $\zeta_a/\zeta$  vs.  $\zeta^*$  for a positively charged plate, and (d)  $\zeta_a/\zeta$  vs.  $\zeta^*$  for a negatively charged plate.  $\zeta_a^* = \zeta_a/k_B T/e$  and  $\zeta^* = \zeta/k_B T/e$ . For reference,  $k_B T/e$  at room temperature (293K) is 25 mV.

### 3.5 Slip: Conclusions and recommendations

Slip can be of utmost importance in electrokinetic systems; however, detecting its presence is difficult owing to the close coupling between the slip length and the interfacial potential, both of which are typically unknown *a priori*. The complexities involved in these phenomena are closely related to ion condensation and ambiguity in the location of the outer Helmholtz plane [83] – both of these issues lead to additional challenges when linking origins of surface charge to electrokinetic phenomena. Slip most likely is ubiquitous in hydrophobic systems, though the relationship between slip and any measurable quantification of hydrophobicity (*e.g.* contact angle) is unclear. The presence of dissolved gases has consistently been shown to affect slip, possibly through interfacial gas/vapor layers (to be discussed further in Section 4).

Slip is especially important in electrokinetic systems, owing to the high shear rates present in the double layer during electroosmosis, and the sensitivity of electrical currents to fluid motion near the channel wall in streaming potential. We have shown through simple analytical/numerical calculations that the presence of slip reduces the applicability of the Debye-Hückel approximation; an effect that is worse for electrolyte ions of larger charge. Furthermore, the slip length,  $b$ , and the electrokinetic potential,  $\zeta$ , are coupled in macroscopically observable electrokinetic phenomena, making their independent measurement difficult.

Since the presence of slip increases the importance of the non-linearity of the Poisson-Boltzmann equation, it may be possible to design experiments where deviations from the Debye-Hückel approximation are measurable. Induced-charged electrokinetic effects may play a role, since they

provide more convenient access to large surface potentials, though these limits also require more advanced double layer modeling [84, 85]. In that case, different electrokinetic phenomena, such as streaming potential and electroosmosis, may exhibit measurably different dependencies on  $b$  and  $\zeta$ . It may also be possible to find surfactants that remove slip from electrokinetic systems, but leave the surface potential unchanged, as was attempted in [24]. More experiments characterizing such surfactants are necessary, though determining their effect on the electrokinetic potential is non-trivial. Owing to the challenges involved, very few attempts have been made to measure slip in electrokinetic systems, but such experiments are necessary in order to better understand the interplay between slip and electrokinetics.

## 4 Interfacial water structure

Both the molecular ( $\sim 1$  Å) and nanofluidic ( $\sim 1$ –100 nm) structure of water at hydrophobic interfaces are related to the electrokinetic performance of microfluidic devices through their roles in interfacial slip, chemistry, and adsorption. For hydrophobic substrates in particular, water structuring effects may even dominate the surface properties, *e.g.*, interfacial charge, slip, and viscosity [86], in which case they would also dominate the electrokinetic response of the system. Macroscopic thermodynamic modeling suggests that changes in entropy drive the formation of ordered water structures at hydrophobic interfaces [87], and that such structures can facilitate preferential adsorption of ions [88, 89]. In the context of slip in hydrophobic microfluidic devices, the interfacial structure has been described in terms of a vapor/gas layer or a layer of depleted water density [68, 69]. Data from recent AFM experiments supports an alternative description, where instead of a continuous gas layer, there exist unstable gaseous nanobubbles at the hydrophobic interface [90].

### 4.1 Depletion layers

When examining slip in hydrophobic systems, Ruckenstein *et al.* [68] considered the possibility of a gaseous gap existing between the solid surface and the liquid due to partial or complete dewetting, rather than treating the molecules of liquid as slipping directly on the channel wall. This idea was later extended to include the role of dissolved gases in determining the size and density of the gap [69, 70], and generalized into a notion of a boundary layer of depleted liquid density (Fig. 4a) [8]. This depletion layer would have a lower viscosity than the bulk solution (leading to apparent slip as described by Eq. 8), but need not be an essentially frictionless liquid-gas interface. In addition to introducing apparent slip, the existence of a depletion layer also alters the surface chemistry and ion adsorption [86], which could lead to some of the ion concentration effects measured at air water interfaces discussed in [1].

X-ray reflectivity [62, 63, 91], neutron reflectivity [60, 61, 92], and AFM [93] experiments have been used to observe depletion layers at various hydrophobic interfaces, allowing for quantitative estimates of depletion layer thicknesses and densities (Table 1). X-ray reflectivity measurements generally report depletion layer thicknesses on the order of Angstroms, while the neutron reflectivity measurements report thicknesses on the order of nanometers. MD simulations [6, 91, 94] tend to agree more closely with the x-ray measurements than with the neutron experiments. Reported depletion layer densities vary in both types of measurement, though there is some ambiguity involved in defining both the thickness and the density. For example, Doshi *et al.* [61] fit their measured density profile to error functions, and defined the depletion layer thickness as the point at which the water density is equal to half the bulk value; Grigera *et al.* [94] examined the angular distribution function of water molecules near the surface, which becomes constant in the bulk. AFM has also been used to measure a depletion layer

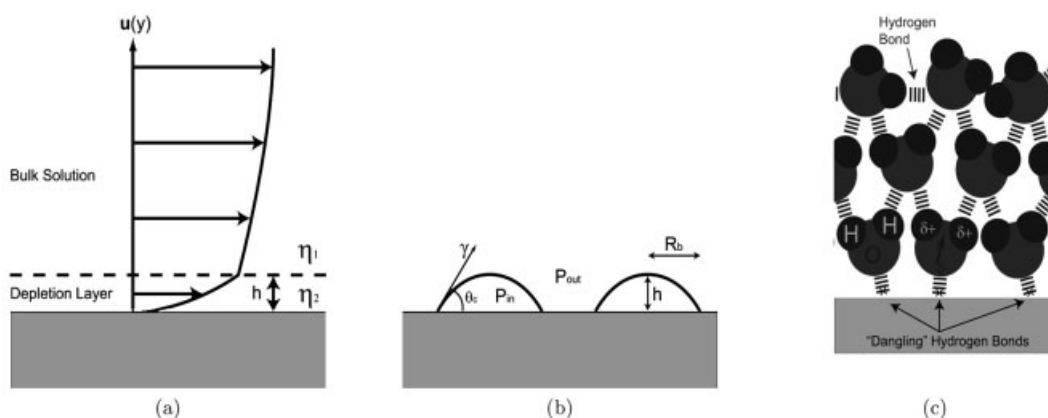


**Figure 4.** Schematics of (a) a depletion layer, (b) roughly hemispherical nanobubbles, and (c) structuring of water on hydrophobic microfluidic substrates. In (c), the dipole moment direction on a representative water molecule is indicated by an arrow.

**Table 1.** Summary of depletion layer measurements

|   | Interface   | Contact Angle | Depletion layer thickness (A) | $\frac{P_{\text{depletion layer}}}{P_{\text{bulk}}}$ |
|---|---|---------------|-------------------------------|--|
| Jensen <i>et al.</i> [91]:<br>X-ray reflectivity and MD | Water-paraffin  | 112°          | 15                            | 0.9  |
| Poynor <i>et al.</i> [62]:<br>X-ray reflectivity        | Water on methylterminated octadecyl silane monolayers | > 100°        | 2-4                           | 0.4  |
| Mezger <i>et al.</i> [63]:<br>X-ray reflectivity        | Water-OTS   | > 100°        | 3.8                           | 0.71   |
| Steitz <i>et al.</i> [92]:<br>Neutron reflectivity      | D <sub>2</sub> O -polystyrene                         | –             | 20-50                         | 0.88-0.94  |
| Schwendel <i>et al.</i> [60]:<br>Neutron reflectivity   | D <sub>2</sub> O on SAMs                              | –             | 41.8                          | 0.869  |
| Doshi <i>et al.</i> [61]:<br>Neutron reflectivity       | D <sub>2</sub> O -OTS                                 | 100.7-113.4°  | 28-35                         | 0.5  |
| Knoben <i>et al.</i> [93]:<br>AFM                       | Stearylated silica in water                           | 100-110°      | 10 nm                         | –  |
| Mamatkulov <i>et al.</i> [6]:<br>MD                     | SPC/E-water model with hydrophobic alkane slab        | –             | 2.5                           | –  |
| Grigera <i>et al.</i> [94]:<br>MD                       | SPC/E-water model with a wall of neutral atoms        | –             | 4                             | –  |

thickness of 10 nm for stearylated silica particles in water [93], but AFM gives no information about the density. For water-octadecyl trichlorosilane (OTS) interfaces, Mezger *et al.* [63] also explored the effect of dissolved gases (Ar, Xe, Kr, N<sub>2</sub>, O<sub>2</sub>, CO, CO<sub>2</sub>, and HCl), and concluded that they did not significantly influence the depletion layer. Doshi *et al.* however, also worked with OTS interfaces, and found that the depletion layer thickness varied across Ar-treated, CO<sub>2</sub>-treated, degassed and naturally aerated solutions, though the variations were not more than 25%. Observation of the existence of a depletion layer even in degassed solutions [61–63] is quite significant, because it suggests that dissolved gases are not required for dewetting, and that the depletion layer is inherent to water-hydrophobe interfaces. Thus understanding of micro/nanofluidics in hydrophobic substrates requires careful attention to these non-uniform fluid density effects at the interface.

## 4.2 Nanobubbles

Nanobubbles, irregular networks of unstable gas bubbles approximately 30 nm in height and 100-300 nm in radius (Fig. 4b), are an alternative (though not necessarily contradictory) description of the structure of hydrophobic interfaces [9]. The existence of nanobubbles at water-hydrophobe interfaces was initially postulated to explain the long-range (10-100 nm) attraction observed between two hydrophobic surfaces, where the attractive force as a function of separation distance was found to have large step changes [95, 102]. These step changes are attributed to the coalescence of nanobubbles, and the magnitude of the expected attractive force change resulting from a bridging event has been shown

to be thermodynamically consistent with experimental observations [95, 103].

Though nanobubbles are compelling in light of the hydrophobic force measurements, they are controversial owing to the fact that their thermodynamic stability requires nanocavities, double layer interactions, diffusive non-equilibrium, or a breakdown in the applicability of classical descriptions of surface tension and its effects via the Young-Laplace equation. The Young-Laplace equation gives the relationship between a bubble's size and its internal pressure.

$$P_{\text{in}} = P_{\text{out}} + \frac{2\gamma}{R_b} \quad (14)$$

where  $P_{\text{in}}$  and  $P_{\text{out}}$  are the pressures inside and outside of the bubble respectively,  $\gamma$  is the surface tension, and  $R_b$  is the radius of curvature of the nanobubble. Thus, a nanobubble 10 nm in radius requires an internal pressure of about 144 atm, meaning that it cannot be in equilibrium with the atmosphere, and is expected to dissolve very quickly. An estimate of the time scale for the dissolution of nanobubbles is given by the time scale for diffusion of a spherical gas bubble into the liquid [104, 105].

$$\tau \sim \frac{Mp_0a^2}{Dc_0RT} \left( 1 + \frac{p_0R_b}{\gamma} \right) \quad (15)$$

where  $M$  is the molar mass,  $p_0$  is the far field pressure,  $D$  is the diffusion coefficient of the gas in the liquid,  $c_0$  is the concentration of the gas,  $T$  is the temperature,  $R$  is the gas constant,  $R_b$  is the radius of the bubble, and  $\gamma$  is the surface tension. Lauga *et al.* [4] point out that  $\tau \approx 10 \mu\text{s}$  for  $R_b =$

10 nm, though it is important to realize that Eqs. (14) and (15) strictly apply for a gas bubble surrounded by fluid in equilibrium with the atmosphere; they do not take into account the presence of a hydrophobic surface, which through surface interactions may slow the kinetics of dissolution. Nevertheless, nanobubbles have experimentally been shown to be stable for much longer than expected. One possible explanation is offered by Attard *et al.* [9, 95, 98, 103], who showed that if the bubbles are not in diffusive equilibrium with the atmosphere over macroscopically observable timescales (*i.e.* they are in a supersaturated solution), the nanobubbles can be thermodynamically stable, and should be modeled using an isobaric chemical potential (fixed number of gas molecules) rather than the grand potential (global equilibrium). For this to be possible, they further proposed that the nanobubbles are in equilibrium with a locally supersaturated solution, though the origin of the supersaturation is unclear. Attard *et al.* also showed that it is thermodynamically feasible for the interfacial structures to instead take the form of supramolecular vapor voids, a description supported by Ljunggren *et al.* [105]. Experiments show the bubbles/voids to be stable for hours, which could be indicative of a diffusion limited process. The presence of nanocavities allow nanoscale gas regions to exist without nanoscale curvature, which further explains nanobubble stability. The microscale analogy of nanocavities is superhydrophobic surfaces [106].

Perhaps the most compelling evidence for the existence of nanobubbles comes from direct observation of water-hydrophobe interfaces with tapping mode AFM [9, 59, 90, 92, 107–110]. Hydrophobic surfaces in water have distinct roughness features, which are absent in dry hydrophobic or wet hydrophilic surfaces. Phase AFM images reveal that the roughness features consist of a much softer material than the bulk substrate [9]. Furthermore, the roughness features are not observable with contact mode AFM imaging, suggesting that the force applied in contact mode destroys or displaces these roughness features. These roughness features have thus been postulated to be gas nanobubbles. Typical values for nanobubble morphology are summarized in Table 2. Descriptions of the general features of nanobubble morphology have differed among different investigators. Attard's group has generally observed bubbles of irregular cross-section [9, 90, 107], while others have observed

hemispherical objects of regular circular cross-section [59, 92, 108–110]. Both descriptions may be correct, as the nanobubble morphology is likely to be a function of both the solution conditions and the substrate material. For example, experiments by Tyrrell *et al.* [107] showed that nanobubble morphology varies as a function of solution pH. At pH 3, the bubbles coalesced into larger regular structures, while at pH 9.4, the mean area of the bubbles was reduced and the distinction between nanobubble domains was enhanced. They propose that this is likely due to enhanced surface charge on the bubbles at higher pH, leading to stabilization due to electrostatic repulsion.

Examination of the role of dissolved gases [96, 99, 102, 110, 111] on the formation and morphology of nanobubbles may elucidate information about their composition (gas *vs.* vapor), and may also help determine the effect of nanobubbles on the performance of electrokinetically driven microfluidic devices. Measurements of the hydrophobic force with AFM/SFA have shown that its range decreases in degassed solutions [96, 99, 102, 111]. Using an optical cavitation method, Vinogradova *et al.* [112] found that the addition of dissolved gases enhances nucleation of nanobubbles on hydrophobic surfaces. This contradicts the findings of Ishida *et al.* [102], who found with AFM measurements of OTS on Si substrates that dissolved gases had no effect on the range of the hydrophobic force. However, they also found that surfaces that were not exposed to air before they were immersed in water and measured with AFM did not have nanobubbles, while surfaces which had been exposed to air prior to measurement did [59]. Zhang *et al.* [110] compared tapping mode AFM images of water-mica interfaces taken with non-degassed and degassed solutions, and found that the nanobubble density decreased from 2.9 *per*  $\mu\text{m}^2$  to nearly zero with degassing. Further study is required in this area in order to draw conclusions about the composition of nanobubbles, but it is clear that exposure to air and/or dissolved gases leads to nanobubble morphology changes, which can lead to uncertainties in electrokinetic actuation in hydrophobic microfluidic devices.

As with depletion layers, nanobubbles can drastically affect the electrokinetic performance of microfluidic devices by introducing a slip boundary condition and altering the surface chemistry. Lauga *et al.* [4, 71, 72] have modeled the effect of nanobubbles on slip, and point out three key differ-

**Table 2.** Summary of AFM nanobubble measurements

|                                    | Interface              | Bubble radius of curvature (nm) | Bubble height (nm) |
|------------------------------------|------------------------|---------------------------------|--------------------|
| Ishida <i>et al.</i> [59]          | Water-OTS              | 220–600                         | 38                 |
| Tyrrell <i>et al.</i> [9, 90, 107] | Water-methylated glass | 100–300                         | 20–30              |
| Lou <i>et al.</i> [108]            | Water-graphite         | –                               | –                  |
| Steitz <i>et al.</i> [92]          | Water-polystyrene      | 25–60                           | 20                 |
| Simonsen <i>et al.</i> [109]       | Water-polystyrene      | 66.7                            | 6.6                |
| Zhang <i>et al.</i> [110]          | Water-mica             | –                               | –                  |

ences between nanobubbles and depletion layers. First, the flow inside nanobubbles recirculates, decreasing the slip length estimate given by Eq. (8). Second, no-slip regions between the bubbles decrease slip further. Third, nanobubbles are generally not flat, which decreases the slip further. In addition, owing to instabilities and coalescence, nanobubbles are dynamic, which means that their formation and dissolution over time will lead to transients in the electrokinetic response of a system. This can be crucial in hydrophobic microfluidic devices, since solvent and/or temperature changes can lead to the nucleation and dissolution of nanobubbles.

### 4.3 Hydrogen-bonded water molecule networks

The structure of water at the interface is likely to dominate the thermodynamics of binding events for ion adsorption onto hydrophobic surfaces in aqueous media [5, 87]. In addition to the macroscopic (depletion layers) and supra-molecular (nanobubbles) structures which have already been discussed, the molecular structure of water at hydrophobic surfaces has been shown to impact both slip and ion adsorption [5–7, 89, 113–116]. Using MD simulations, Lee *et al.* [113] showed that water forms an oriented ice-like structure at extended hydrophobic surfaces. The molecules nearest to the surface are oriented such that only one hydrogen bonding group faces the surface, an arrangement referred to as dangling hydrogen bonds (Fig. 4c). This structure results from the competition between the tendencies of the liquid to maximize hydrogen bonds, and to maximize packing density. Zangi *et al.* [7] further showed that the ordered structure leads to an electrical potential gradient that strongly and favorably interacts with the dipole moments of hydroxyl ions, leading to their spontaneous adsorption. Additional MD studies have shown that oriented water molecules can also stabilize adsorbed ions, and that the dynamics of ion hydration play a significant role during an electrolyte ion's approach to a hydrophobic surface [5, 6, 114]. Mamatkulov *et al.* [6] observed the formation of a depletion layer as a result of the water's molecular structure, relating the structure of water at the hydrophobic interface to slip phenomena.

The tendency of water to form ordered hydrogen-bonded structures near extended hydrophobic surfaces has been confirmed experimentally through spectroscopic measurements of air-water interfaces [89, 115, 116]. Raduge *et al.* [115] used sum frequency generation (SFG) to observe the interface between air and aqueous sulfuric acid. They reported three characteristic peaks at  $3670\text{ cm}^{-1}$ ,  $3200\text{ cm}^{-1}$  and  $3400\text{ cm}^{-1}$ , which correspond to dangling OH bonds at the surface, hydrogen bonded OH groups associated with ice-like structures, and less ordered local bonding structures respectively. As they increased the  $\text{H}_2\text{SO}_4$  concentration, they found that the  $3670\text{ cm}^{-1}$  peak disappeared, which they attributed to the interaction of  $\text{H}_2\text{SO}_4$  molecules with the dangling OH groups. Baldelli *et al.* [116] obtained similar results,

but interpreted them differently, stating that ionic species tend to orient water molecules into ordered structures more than in the neat air-water interface. Using SFG and ATR-FTIR (attenuated total reflection Fourier transform infrared) spectroscopy, Liu *et al.* [89] demonstrated that different ions can affect the hydrogen bonded water structure differently. The water structure in the presence of smaller ions such as F and Cl is very similar to that of the neat air-water interface, while larger ions such as Br and I tend to distort the hydrogen bonded network significantly. Consequently, Liu *et al.* also observed enhanced concentration of the larger ions only, suggesting that the distortion and/or reorientation of the hydrogen bonded network plays a crucial role in preferential ion adsorption. This is critical in microfluidics, as it affects the surface charge, and ultimately the electrokinetic performance of hydrophobic devices.

### 4.4 Interfacial water structure: Conclusions and recommendations

Interfacial charge formation and slip on hydrophobic surfaces are likely to be dependent on (i) the structure of water at the interface, and (ii) the presence of dissolved gases. The existence of ordered water structures at hydrophobic interfaces is predicted by MD simulations [5–7], which are in good agreement with spectroscopic experiments [89, 115, 116]. The impact of these structures on interfacial charge formation is an area that warrants further investigation. MD simulations have shown that ordered water structures can facilitate adsorption of hydroxyl ions [7], though to the authors' knowledge, direct experimental evidence for ordered water structuring is lacking. The distortion of these water structures has been shown *via* spectroscopic measurements to correspond with preferential anion adsorption [89]; future investigations here should be focused on thermodynamic modeling of these systems.

Observed regions of depleted water density near the interface are likely to be related to water structuring [6]. From neutron/X-ray reflectivity [60–63, 91, 92] and AFM [93] experiments, the characteristics of the depletion layer appear to be only marginally affected by the presence of dissolved gases, if at all. These depletion regions are also generally observed regardless of whether solutions are degassed. Though the composition of the depletion layer is essentially unknown, these data suggest that the depletion region is better described as a vapor layer, rather than as a gas layer. In either case, the fluid in the depletion region has properties that differ from their bulk values (*e.g.*, viscosity, permittivity); this lends credibility to the postulate that a low viscosity layer near the interface leads to slip. Nanobubbles are likely to exist at hydrophobic interfaces in addition to the depletion region, though unlike depletion layers, they tend to be less prolific in degassed solutions [59, 96, 99, 102, 111]. This suggests that the bubbles are more likely to contain gas rather than vapor, though their composition is also uncharacterized at this point. Future experiments should focus on

determining the composition of these interfacial structures either spectroscopically or chemically. Nanobubbles also introduce slip at the interface, though there are fundamental differences between depletion layers and nanobubbles in this respect, as discussed in [4].

Since nanobubbles are unstable, and likely to be linked with slip and interfacial charge, they are expected to lead to transients in the macroscopically observable properties of hydrophobic microfluidic systems as they form/dissolve over time. Thus, it would be interesting to see how changes in the molecular/nanofluidic structures at water-hydrophobe interfaces correspond to changes in the macroscopic properties of the system when the input parameters (*i.e.* pH, ionic strength, *etc.*) are varied, and over time.

## 5 Concluding remarks

It has been shown that the complex interplay between diffuse interfacial structures, interfacial chemistry, and slip phenomena result in electrokinetic behavior that is difficult to predict, and is highly dependent on both the solvent and the electrolytes considered. Despite the general complexity of these systems and a dearth of firm and rigorous conclusions, several noteworthy trends have been demonstrated.

Given interfacial charge and the attendant zeta potential as discussed in [1], we discuss the impact of interfacial slip on microdevice performance. The presence of slip can be crucial in hydrophobic electrokinetic systems, due to the presence of high shear rates owing to the localization of shear to the double layer. Electrokinetic measurements in the presence of slip are especially difficult, since the slip length and electrokinetic potential are coupled in macroscopically observable phenomena, and both are unknown *a priori*. The concentration of dissolved gas in solution has consistently been shown to affect slip, suggesting that presence of gas or vapor at the interface could be the fundamental origin of slip. Given the important roles of dissolved gases in many bio-analytical systems, most microdevices will use working solutions with dissolved gases, and the effects of these gases, especially when perturbed by experimental protocols, must be taken into account. Through simple analytical and numerical calculations, we have shown that slip in electrokinetic systems also limits the applicability of the Debye-Hückel approximation. The Debye-Hückel approximation fails at lower  $\zeta$ -potentials in systems with larger slip lengths; this effect worsens with ions of larger valence.

Both slip and interfacial charge are likely to be affected by interfacial nanostructures on molecular or supramolecular scale. Hydrogen-bonded water networks at hydrophobic interfaces, which are important in both electrolyte and hydroxyl ion interfacial adsorption [1], may also correspond with a region of depleted water density at the interface, which has reduced viscosity when compared to the bulk solution, and generates an apparent slip boundary condition on the fluid velocity. Nanobubbles observed at these interfaces

have a peculiarly slow dissolution rate, given their classically predicted instability. Thus the thermodynamics of nanobubble formation/dissolution are particularly interesting and challenging, though not currently well understood. Nanobubble dynamics are of critical interest when considering design of electrokinetic systems, as the dissolution of nanobubbles over time will lead to transient electrokinetic behavior owing to changes in surface chemistry and slip.

*The authors have declared no conflict of interest.*

## 6 References

- [1] Tandon, V., Bhagavatula, S. K., Nelson, W. C., Kirby, B. J., *Electrophoresis* 2007, 28, this issue.
- [2] Gun'ko, V. M., Turov, V. V., Bogatyrev, V. M., Zarko, V. I., *Adv. Colloid Interface Sci.* 2005, 118, 125–172.
- [3] Teschke, O., Ceotto, G., de Souza, E. F., *Chem. Phys. Lett.* 2000, 326, 328–334.
- [4] Lauga, E., Brenner, M. P., Stone, H. A., *Handbook of Experimental Fluid Dynamics*, Springer, New York, 2005.
- [5] Dang, L. X., Chang, T., *J. Phys. Chem. B* 2002, 106, 235–238.
- [6] Mamatkulov, S. I., Khabibullaev, P. K., Netz, R. R., *Langmuir* 2004, 20, 4756–4763.
- [7] Zangi, R., Engberts, J. B. F. N., *J. Am. Chem. Soc.* 2005, 127, 2272–2276.
- [8] Vinogradova, O. I., *Langmuir* 1995, 11, 2213–2220.
- [9] Attard, P., Moody, M. P., Tyrell, J. W. G., *Physica A* 2002, 314, 696–705.
- [10] Hunter, R. J., *Foundations of Colloid Sci., Vol. 2*, Clarendon Press, Oxford, 1989.
- [11] Huang, X., Gordon, M. J., Zare, R. N., *Anal. Chem.* 1988, 60, 1837–1838.
- [12] Lukacs, K. D., Jorgenson, J. W., *J. High Resolut. Chromatogr.* 1985, 8, 407–411.
- [13] Schutzner, W., Kenndler, E., *Anal. Chem.* 1992, 64, 1991–1995.
- [14] Locascio, L. E., Perso, C. E., Lee, C. S., *J. Chromatogr. A* 1999, 857, 275–284.
- [15] Ocvirk, G., Munroe, M., Tang, T., Oleschuk, R., Westra, K., Harrison, D. J., *Electrophoresis* 2000, 21, 107–115.
- [16] Reijenga, J. C., Aben, G. V. A., Verheggen, T. P. E. M., Everaerts, F. M., *J. High Resolut. Chromatogr.* 1983, 8, 407–411.
- [17] Werner, C., Korber, H., Zimmermann, R., Dukhin, S., Jacobasch, H., *J. Colloid Interface Sci.* 1998, 208(1), 329–346.
- [18] Lappan, U., Buchhammer, H.-M., Lunkwitz, K., *Polymer* 1999, 40, 4087–4091.
- [19] Mela, P., van den Berg, A., Fintschenko, Y., Cummings, E. B., *et al.*, *Electrophoresis* 2005, 26, 1792–1799.
- [20] Stone, H. A., Stroock, A. D., Ajdari, A., *Ann. Rev. Fluid Mech.* 2004, 36, 381–411.
- [21] Squires, T. M., Quake, S. R., *Rev. Mod. Phys.* 2005, 77, 977–1026.
- [22] Boehnke, U.-C., Remmler, T., Motschmann, H., Wurlitzer, S., *et al.*, *J. Colloid Interface Sci.* 1999, 211, 243–251.

- [23] Choi, C-H., Johan, K., Westin, A., Breuer, K. S., *Phys. Fluids* 2003, 15, 2897–2902.
- [24] Churaev, N. V., Ralston, J., Sergeeva, I. P., Sobolev, V. D., *Adv. Colloid Interface Sci.* 2002, 96, 265–278.
- [25] Churaev, N. V., Sobolev, V. D., Somov, A. N., *J. Colloid Interface Sci.* 1984, 97, 574–581.
- [26] Henry, C. L., Neto, C., Evans, D. R., Biggs, S., Craig, V. S. J., *Physica A* 2004, 339, 60–65.
- [27] Joseph, P., Tabeling, P., *Phys. Rev. E* 2005, 71, 035303.
- [28] Hervet, H., Leger, L., *C.R. Physique* 2003, 4, 241–249.
- [29] Tretheway, D. C., Meinhart, C. D., *Phys. Fluids* 2002, 14, L9–L12.
- [30] Tretheway, D. C., Meinhart, C. D., *Phys. Fluids* 2004, 16, 1509–1515.
- [31] Vinogradova, O. I., Yakubov, G. E., *Langmuir* 2003, 19, 1227–1234.
- [32] Baudry, J., Charlaix, E., Tonck, A., Mazuyer, D., *Langmuir* 2001, 17, 5232–5236.
- [33] Cheikh, C., Koper, G., *Phys. Rev. Lett.* 2003, 91, 156102.
- [34] Cho, J. J., Law, B. M., Rieutord, F., *Phys. Rev. Lett.* 2004, 92, 166102.
- [35] Kisleva, O. A., Sobolev, V. D., Churaev, N. V., *Colloid J.* 1999, 61, 263–264.
- [36] Lumma, D., Best, A., Gansen, A., Feuillebois, F. et al., *Phys. Rev. E* 2003, 67, 056313.
- [37] Sun, G., Bonaccorso, E., Franz, V., Butt, H.-J., *J. Chem. Phys.* 2002, 117, 10311–10314.
- [38] Zhu, Yingxi, Granick, S., *Phys. Rev. Lett.* 2002, 88, 106102.
- [39] Zhu, Y., Granick, S., *Langmuir* 2002, 18, 10058–10063.
- [40] Navier, C. L. M. H., *Memoire sur les lois du mouvement des fluides*, Mem. Acad. R. Sci., France, 1823.
- [41] Maxwell, J. C., *Philosophical Transactions of the Royal Soc. of London* 1879, 170, 231–256.
- [42] Pfahler, J., Harley, J., Bau, H., Zemel, J., *Sens. Actuators A21* –A23, 1990, 431–434.
- [43] Hasegawa, T., Suganuma, M., Watanabe, H., *Phys. Fluids* 1997, 9, 1–3.
- [44] Cheng, J. T., Giordano, N., *Phys. Rev. E* 2002, 65, 031206.
- [45] Israelachvili, J. N., Adams, G. E., *J. Chem. Soc. Faraday Trans. I* 1978, 74, 975–1001.
- [46] Israelachvili, J. N., *J. Colloid Interface Sci.* 1986, 110, 263–271.
- [47] Vinogradova, O. I., Yakubov, G. E., Butt, H.-J., *J. Chem. Phys.* 2001, 114, 8124–8131.
- [48] Bonaccorso, E., Kappl, M., Butt, H.-J., *Phys. Rev. Lett.* 2002, 88, 076103.
- [49] Bonaccorso, E., Butt, H.-J., Craig, V. S. J., *Phys. Rev. Lett.* 2003, 90, 144501.
- [50] Vinogradova, O. I., *Langmuir* 1996, 12, 5963–5968.
- [51] Vinogradova, O. I., *J. Phys. – Condens. Matter* 1996, 8, 9491–9495.
- [52] Vinogradova, O. I., *Langmuir* 1998, 14, 2827–2837.
- [53] Vinogradova, O. I., Horn, R. G., *Langmuir* 2001, 17, 1604–1607.
- [54] Israelachvili, J. N., Tabor, D., *Proc. Royal Soc. Lond. A* 1972, 331, 19–38.
- [55] Zettner, C. M., Yoda, M., *Exp. Fluids* 2003, 34, 115–121.
- [56] Sadr, R., Yoda, M., Zheng, Z., Conlisk, A. T., *J. Fluid Mech.* 2004, 506, 357–367.
- [57] Jabberzadeh, A., Atkinson, J. D., Tanner, R. I., *Phys. Rev. E* 2000, 61, 690–699.
- [58] Georges, J. M., Millot, S., Loubet, J. L., Tonck, A., *J. Chem. Phys.* 1993, 98, 7345–7360.
- [59] Ishida, N., Inoue, T., Miyahara, M., Higashitani, K., *Langmuir* 2000, 16, 6377–6380.
- [60] Schwendel, D., Hayashi, T., Dahint, R., Pertsin, A. et al., *Langmuir* 2003, 19, 2284–2293.
- [61] Doshi, D. A., Watkins, E. B., Israelachvili, J. N., Majewski, J., *PNAS* 2005, 102, 9458–9462.
- [62] Poynor, A., Hong, L., Robinson, I. K., Granick, S. et al., *Phys. Rev. Lett.* 2006, 97, 266101.
- [63] Mezger, M., Reichert, H., Schoeder, S., Okasinski, J. et al., *PNAS* 2006, 103, 18401–18404.
- [64] Craig, V. S. J., Neto, C., Williams, D. R. M., *Phys. Rev. Lett.* 2001, 87, 054504.
- [65] Neto, C., Craig, V. S. J., Williams, D. R. M., *Eur. Phys. J. E* 2003, 12, S71–S74.
- [66] Zhu, Y., Granick, S., *Phys. Rev. Lett.* 2001, 87, 096105.
- [67] Zhu, Y., Granick, S., *Macromolecules* 2002, 35, 4658–4663.
- [68] Ruckenstein, E., Churaev, N., *J. Colloid Interface Sci.* 1983, 96, 488–491.
- [69] Ruckenstein, E., Churaev, N., *J. Colloid Interface Sci.* 1991, 147, 535–538.
- [70] de Gennes, P. G., *Langmuir* 2002, 18, 3413–3414.
- [71] Lauga, E., Stone, H. A., *J. Fluid Mech.* 2003, 489, 55–77.
- [72] Lauga, E., Brenner, M. P., *Phys. Rev. E* 2004, 70, 026311.
- [73] Granick, S., Zhu, Y., Lee, H., *Nature Materials* 2003, 2, 221–227.
- [74] Tretheway, D. C., Stone, S., Meinhart, C. D., *Bull. Am. Phys. Soc.* 2004, 49, 215.
- [75] Sato, H., Matubayasi, N., Nakahara, M., Hirata, F., *Chem. Phys. Lett.* 2000, 323, 257–262.
- [76] Anderson, G. K., *J. Chem. Thermodynamics* 2003, 35, 1171–1183.
- [77] Khan, A., *J. Mol. Struct. (Thermochem)* 2003, 664–665, 237–245.
- [78] Yang, J., Kwok, D. Y., *J. Phys. Chem. B* 2002, 106, 12851–12855.
- [79] Yang, J., Kwok, D. Y., *J. Colloid Interface Sci.* 2003, 260, 225–233.
- [80] Yang, J., Kwok, D. Y., *Langmuir* 2003, 19, 1047–1053.
- [81] Yang, J., Kwok, K. Y., *J. Chem. Phys.* 2003, 118, 354–363.
- [82] Joly, L., Ybert, C., Trizae, E., Bocquet, L., *Phys. Rev. Lett.* 2004, 93, 257805.
- [83] Hunter, R. J., *Zeta Potential in Colloid Sci.*, Academic Press, London, 1981.
- [84] Bazant, M. Z., Squires, T. M., *Phys. Rev. Lett.* 2004, 92, 066101.
- [85] Squires, T. M., Bazant, M. Z., *J. Fluid Mech.* 2004, 509, 217–252.
- [86] Netz, R. R., *Curr. Opin. Colloid Interface Sci.* 2004, 9, 192–197.
- [87] Tanford, C., *The Hydrophobic Effect: Formation of Micelles and Biological Membranes*, John Wiley and Sons, New York 1980.

- [88] Marinova, K. G., Alargova, R. G., Denkov, N. D., Velev, O. D., *et al.*, *Langmuir* 1996, 12, 2045–2051.
- [89] Liu, D., Ma, G., Levering, L. M., Allen, H. C., *J. Phys. Chem. B* 2004, 108, 2252–2260.
- [90] Tyrrell, J. W. G., Attard, P., *Phys. Rev. Lett.* 2001, 87, 176104.
- [91] Jensen, T. R., Jensen, M. O., Reitzel, N., Balashev, K., *et al.*, *Phys. Rev. Lett.* 2003, 90, 086101.
- [92] Steitz, R., Gutberlet, T., Hauss, T., Klosgen, B., *et al.*, *Langmuir* 2003, 19, 2409–2418.
- [93] Knoblen, W., Besseling, A. M., Cohen Stuart, M. A., *Langmuir* 2007, 23, 6095–6105.
- [94] Grigera, J. R., Kalko, S. G., Fischbarg, J., *Langmuir* 1996, 12, 154–158.
- [95] Parker, J. L., Claesson, P. M., Attard, P., *J. Phys. Chem.* 1994, 98, 8468–8480.
- [96] Meagher, L., Craig, V. S. J., *Langmuir* 1994, 10, 2736–2742.
- [97] Wood, J., Sharma, R., *Langmuir* 1995, 11, 4797–4802.
- [98] Attard, P., *Langmuir* 1996, 12, 1693–1695.
- [99] Mahnke, J., Stearnes, J., Hayes, R. A., Fornasiero, D., Ralston, J., *Phys. Chem. Chemical Phys.* 1999, 1, 2793–2798.
- [100] Carambassis, A., Jonker, L. C., Attard, P., Rutland, M. W., *Phys. Rev. Lett.* 1998, 80, 5357–5360.
- [101] Yakubov, G. E., Butt, H.-J., Vinogradova, O. I., *J. Phys. Chem. B* 2000, 104, 3407–3410.
- [102] Ishida, N., Sakamoto, M., Miyahara, M., Higashitani, K., *Langmuir* 2000, 16, 5681–5687.
- [103] Attard, P., *Langmuir* 2000, 16, 4455–4466.
- [104] Epstein, P. S., Plesset, M. S., *J. Chem. Phys.* 1950, 18, 1505–1509.
- [105] Ljunggren, S., Eriksson, J. C., *Colloids Surf. A* 1997, 130, 151–155.
- [106] Ma, M., Hill, R. M., *Curr. Opin. Colloid Interface Sci.* 2006, 11, 193–202.
- [107] Tyrrell, J. W. G., Attard, P., *Langmuir* 2002, 18, 160–167.
- [108] Lou, S., Gao, J., Xiao, X., Li, X., *et al.*, *Materials Characterization* 2002, 48, 211–214.
- [109] Simonsen, A. C., Hansen, P. L., Klosgen, B., *J. Colloid Interface Sci.* 2004, 273, 291–299.
- [110] Zhang, X. H., Zhang, X. D., Lou, S. T., Zhang, Z. X., *et al.*, *Langmuir* 2004, 20, 3813–3815.
- [111] Considine, R. F., Hayes, R. A., Horn, R. G., *Langmuir* 1999, 15, 1657–1659.
- [112] Vinogradova, O. I., Bunkin, N. F., Churaev, N. V., Kisleva, O. A., *et al.*, *J. Colloid Interface Sci.* 1995, 173, 443–447.
- [113] Lee, C. Y., McCammon, J. A., Rossky, P. J., *J. Chem. Phys.* 1984, 80, 4448–4455.
- [114] Vrbka, L., Mucha, M., Minofar, B., Jungwirth, P., *Current Opin. Colloid Interface Sci.* 2004, 9, 67.
- [115] Raduge, C., Pflumio, V., Shen, Y. R., *Chem. Phys. Lett.* 1997, 274, 140–144.
- [116] Baldelli, S., Schnitzer, C., Schultz, M., Campbell, D. J., *Chem. Phys. Lett.* 1998, 287, 143–147.